Maghsoudi, S., Cesca, S., Hainzl, S., Kaiser, D., Becker, D., Dahm, T. (2013): Improving the estimation of detection probability and magnitude of completeness in strongly heterogeneous media, an application to acoustic emission (AE). - Geophysical Journal International, 193, 3, pp. 1556—1569.

DOI: http://doi.org/10.1093/gji/ggt049

Geophysical Journal International

Geophys. J. Int. (2013) **193,** 1556–1569
Advance Access publication 2013 March 08

doi: 10.1093/gji/ggt049

Improving the estimation of detection probability and magnitude of completeness in strongly heterogeneous media, an application to acoustic emission (AE)

Samira Maghsoudi,[1] Simone Cesca,[1,2] Sebastian Hainzl,[2] Diethelm Kaiser,[3] Dirk Becker[4] and Torsten Dahm[2]

[1] *Institute of Earth and Environmental Sciences, University of Potsdam, Germany. E-mail: Samira.Maghsoudi@geo.uni-potsdam.de*
[2] *GFZ Potsdam, Germany*
[3] *BGR Hannover, Germany*
[4] *University of Hamburg, Germany*

Accepted 2013 February 5. Received 2013 February 4; in original form 2012 March 01

SUMMARY

Reliable estimations of magnitude of completeness (M_c) are essential for a correct interpretation of seismic catalogues. The spatial distribution of M_c may be strongly variable and difficult to assess in mining environments, owing to the presence of galleries, cavities, fractured regions, porous media and different mineralogical bodies, as well as in consequence of inhomogeneous spatial distribution of the seismicity. We apply a 3-D modification of the probabilistic magnitude of completeness (PMC) method, which relies on the analysis of network detection capabilities. In our approach, the probability to detect an event depends on its magnitude, source–receiver Euclidian distance and source–receiver direction. The suggested method is proposed for study of the spatial distribution of the magnitude of completeness in a mining environment and here is applied to a 2-months acoustic emission (AE) data set recorded at the Morsleben salt mine, Germany. The dense seismic network and the large data set, which includes more than one million events, enable a detailed testing of the method. This method is proposed specifically for strongly heterogeneous media. Besides, it can also be used for specific network installations, with sensors with a sensitivity, dependent on the direction of the incoming wave (e.g. some piezoelectric sensors). In absence of strong heterogeneities, the standards PMC approach should be used. We show that the PMC estimations in mines strongly depend on the source–receiver direction, and cannot be correctly accounted using a standard PMC approach. However, results can be improved, when adopting the proposed 3-D modification of the PMC method. Our analysis of one central horizontal and vertical section yields a magnitude of completeness of about $M_c \approx 1$ (AE magnitude) at the centre of the network, which increases up to $M_c \approx 4$ at further distances outside the network; the best detection performance is estimated for a NNE–SSE elongated region, which corresponds to the strike direction of the low-attenuating salt body. Our approach provides us with small-scale details about the capability of sensors to detect an earthquake, which can be linked to the presence of heterogeneities in specific directions. Reduced detection performance in presence of strong structural heterogeneities (cavities) is confirmed by synthetic waveform modelling in heterogeneous media.

Key words: Seismic attenuation; Statistical seismology.

INTRODUCTION

A first outcome of seismic monitoring is the compilation of seismic catalogues for the monitored region. The assessment of earthquake catalogue completeness is essential for statistical analysis of seismicity and to understand the capabilities of recording networks (Schorlemmer & Woessner 2008). The completeness of a catalogue depends on several factors, including network geometry, instrumentation, magnitude and spatiotemporal distribution of seismicity and attenuation of the seismic signals. The magnitude of completeness (M_c) is defined as the lowest magnitude for which all earthquakes with higher magnitudes can be detected (Rydelek & Sacks 1989;

Woessner & Wiemer 2005). A reliable M_c determination is vital for numerous seismicity and hazard-related studies, such as analysis of rate changes, calculation and mapping of seismicity parameters, static and dynamic triggering, probabilistic seismic hazard assessment and earthquake forecasting. If the frequency–magnitude distribution (FMD) of earthquake catalogues obeys the Gutenberg–Richter law (Gutenberg & Richter 1944), M_c can be defined as the minimum magnitude at which the cumulative FMD departs from the linear trend (Zuniga & Wyss 1995).

Seismic networks in mines are located in complex observational volumes, which contain different geological units and cavities. The static and dynamic properties in mines vary strongly in space (Cichowicz *et al.* 1988; Milev & Spottiswoode 2002). Local heterogeneities influence the seismic wave field in mines significantly and the very high frequency signals, which are monitored (Maxwell & Young 1998). In mining environments, M_c may therefore show strong spatial variations. A number of statistical techniques are available to compute M_c, most of them assuming the validity of the Gutenberg–Richter law and are based on catalogue data. These methods include goodness-of-fit test—GFT (Wiemer & Wyss 2000), M_c-estimation based on the *b*-value stability—MBS (Cao & Gao 2002), entire magnitude range (EMR) approach (Woessner & Wiemer 2005), maximum curvature technique (MAXC; Wyss *et al.* 1999; Wiemer & Wyss 2000) and median-based analysis of the segment slope (MBASS; Amorèse 2007).

The determination of M_c for larger regions using catalogue-based methods, and neglecting small-scale heterogeneities, may lead to erroneous estimations. Better estimations could be obtained by computing M_c for smaller regions. However, this will decrease the number of available events, and the estimation of M_c may get less accurate or even will be impossible for those cells where the number of events is too small. Furthermore, the application of all these existing approaches relies on several assumptions. Beside the validity of Gutenberg–Richter power-law distribution, which does not always hold, the completeness should be constant within earthquake samples and temporal variations can be neglected, which is both often not true in mining environments (for more details see Schorlemmer & Woessner 2008).

Given these limitations for inhomogeneous catalogues, Schorlemmer & Woessner (2008) proposed an alternative method, namely the probability-based magnitude of completeness (PMC), which uses the phase data, station information and network attenuation relations to estimate earthquake detection probabilities. This method does not assume a power-law behaviour of earthquake magnitudes. It has been applied to different regional networks to assess the spatial distribution of the magnitude of completeness. The proposed PMC method was first applied to assess the spatial distribution of M_c using the southern California seismic network (Schorlemmer & Woessner 2008), and later to different regions and seismic networks (Schorlemmer 2009; Nanjo *et al.* 2010; Schorlemmer *et al.* 2010; Gentili *et al.* 2011). However, the PMC approach is based on the assumption that the probability of detecting an event is only dependent on its magnitude and distance to the sensor. In mining environments, as well as in other regions characterized by strong attenuation anomalies and structural heterogeneities, the expected signal amplitudes and the sensor detection thresholds may significantly vary depending on the direction of the incoming wave front.

Plenkers *et al.* (2011) first applied the PMC analysis to study detection probabilities and completeness in a gold mine, using a network of 8 AE sensors combined with one triaxial accelerometer. The authors proposed to define probability of detection at each sensor, based on magnitude, Euclidian distance, depth and azimuth, and showed that the probability of detection depends on ray paths and is influenced by local heterogeneities. They apply a coarser binning when calculating the 3-D completeness distribution and divide the catalogue into subcatalogues that represent areas of homogeneous completeness.

We propose a different extension of the standard PMC approach, applicable to study strongly heterogeneous environments in larger mine networks, and show its application to an appropriate data set, which allows a detailed comparison and test of the methodology. We analyse the acoustic emission (AE) catalogue from the Morsleben Mine, Saxony-Anhalt, Germany, consisting of more than one million events recorded during 2 months**.** Given the large data set, we are able to consider six preferential directions at each sensor, which have been chosen according to the galleries geometry. We show that the detection probabilities are strongly direction-dependent and that the corresponding M_c estimations are significantly influenced by this fact. Our study demonstrates the importance of taking account of 3-D effects in strongly heterogeneous environments such as mines to get reliable M_c estimations based on PMC network methodology.

AE CATALOGUE, MORSLEBEN SALT MINE

In this work we use AE data recorded in the Morsleben salt mine in eastern Germany. The Morsleben salt mine is located in the Allertal region, it has a length of 5.6 km and maximum width of 1.4 km. Its four main levels reach a depth of 630 m below the surface. Until 1969, the Morsleben salt mine was mainly used for mining of potash and rock salt. During mining, large excavation sites in form of cavities were built, showing typical dimensions of 100 m length, 30 m width and 30 m height. This led to a total cavity volume of 5.8 million m^3. Parts of the mine are used as a permanent repository for low- and intermediate-level radioactive waste. The facility is currently being decommissioned. Details on the Morsleben repository are given, for example, in Behlau & Mingerzahn (2001), Preuss *et al.* (2002) and Federal Office for Radiation Protection (2009). Deformation occurs within the rock masses close to the cavities, leading to the development of microcracks, with dimensions of millimetres to centimetres. These are associated with dilatancy and can lead to an increase of the rock permeability (Spies & Eisenblätter 2001b; Spies *et al.* 2005). During these fracturing processes, high-frequency elastic energy is emitted. The AE monitoring is used to detect and locate microcracks and provide information to control the stability of the cavity system (Eisenblätter & Spies 2000). Fig. 1 shows an East–West cross-section view of cavities distribution and the distribution of AE events with acoustic emission magnitude (M_{AE}) larger than $M_{AE} \geq 3$.

A network of 32 piezoelectric sensors was installed by the Bundesanstalt fur Geowissenschaften und Rohstoffe (BGR) in the mine to monitor AE activity. Sensor records have a sampling rate of 200 kHz, and record in triggered mode. No waveform records are available for this data set, and the only available information is the AE event catalogue containing event location, magnitude, trigger information and automatic *P*- and *S*-wave picks. Event magnitudes are derived from the maximum recorded amplitudes and the distances to the receivers (Köhler *et al.* 2009). The mean amplitude is then defined as the amplitude value of the linear regression curve of amplitude over distance at a reference distance of 50 m from the source (Eisenblätter & Spies 2000). This value is expressed in dB with a reference voltage of 1 μV prior to amplification (Spies & Eisenblätter 2001a,b; Spies *et al.* 2005). No simple conversion

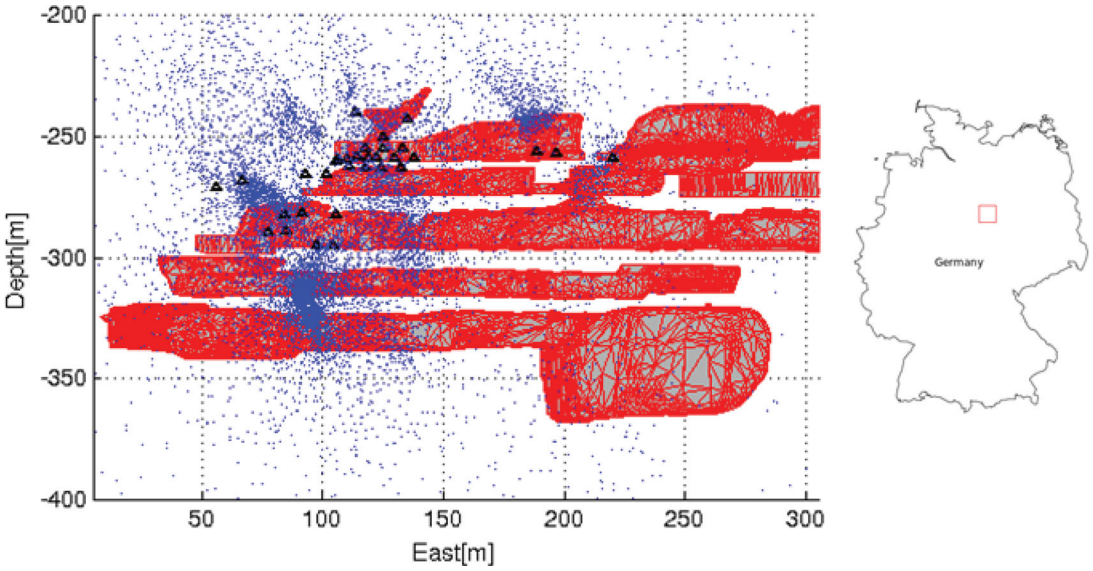

Figure 1. Overview of the study region in the mine and the AE receiver network. East–west cross-section view shows the distribution of cavities (grey and red outlines), the locations of the AE receivers (black triangles) and the distribution of AE activity with a magnitude $M_{AE} \geq 3$.

to commonly used magnitudes like Mw or ML is possible. Scaling relations for these magnitudes are only valid for large or moderate events (Hanks & Boore 1984; Ben-Zion & Zhu 2002), while Kwiatek *et al.* (2011) showed that scaling relations are preserved down to at least magnitude −4.1, when using AE sensors.

Cox & Meredith (1993) suggested that the examination of the distribution of AE event amplitudes may be described by a power law such as the Gutenberg–Richter distribution proposed for earthquake catalogues.

$$\log_{10}(N) = a - bM, \tag{1}$$

where N is the cumulative number of earthquakes with magnitudes larger than M (which is a logarithmic scale of instrumentally recorded amplitudes) and a and b are constants. To produce the same form of the FMD for AE events, amplitudes reported in dB were divided by 20, due to the fact that the AE peak amplitude is measured in dB whereas the earthquake magnitude used in the Gutenberg–Richter distribution is defined in terms of the logarithm of maximum amplitudes. This is a common approach to calculate b-values of AE events which is dimensionless and independent of instrumental sensitivity (e.g. Cox & Meredith 1993; Becker *et al.* 2010).

For our analysis, we use a catalogue of AE-events recorded during 2 months (2010 April–May). During this period, 100 5927 events were detected. Fig. 2 shows the distribution of events which are concentrated close to the network and at the depth range 250–270 m with M_{AE} in the range 0–5. Assuming empirical energy relations (Eisenblätter & Spies 2000), these M_{AE} values result in moment magnitudes $\sim M_w$ −8 up to −3. In this study we derive the 3-D detection probability for each sensor in the network (as a function of magnitude, distance and source-sensor preferential directions) and combine the results from the single sensors to derive 3-D maps of the detection probability and the magnitude of completeness. We focus for visualization on two profiles (a horizontal layer in the depth range of $Z = 253 \pm 5$ m and a cross-section at EW $X = 85 \pm 5$ m), where most sensors are located and the number of recorded events is highest.

Application of most catalogue-based methods needs the assumption that the FMD follows the Gutenberg–Richter law (eq. 1). We analysed the FMD of the whole data set and for different depth profiles, finding in some cases significant deviations from the Gutenberg–Richter power-law distribution. In particular some FMDs show characteristic kinks (see Fig. 3). Therefore, we first investigated whether the anomaly in the FMD distribution might be a consequence of temporal changes in the recording network. However, when considering only events recorded in time periods, with a homogeneous network configuration, we still observe anomalous FMDs. Therefore, we conclude that the deviation from the Gutenberg–Richter law does not stem from temporal changes in the network configuration. We also considered the possibility that the deviations from the Gutenberg–Richter law might result from the superposition of different regions with varying b-values and/or completeness magnitudes. For that purpose, we analysed the FMDs for subvolumes, finding out that the kinks appear only in some cells. Multimodal FMDs have been often observed in mining environments (e.g. Gibowicz & Kijko 1994), who suggested some physical reasons to explain these features. A reasonable hypothesis is that they are the results of strong structural inhomogeneities, such as cavities or different geological bodies, which affect the small-scale distribution of the medium properties, local stresses and stress rates. In our case, the observation of kinks in the FMDs would suggest that the spatial scale of these anomalies is smaller than our resolution power. Because of the deviations from the Gutenberg–Richter distribution, which is observed for many cells, the application of catalogue-based approach for the whole mine cannot provide reliable estimations of M_c in our case. The Gutenberg–Richter law may be satisfied for smaller cells, but this would reduce the number of events per cell and thus limit the application of catalogue-based methods.

NETWORK-BASED METHOD TO ESTIMATE M_c

The probabilistic magnitude of completeness (PMC) method was developed to analyse detection probability of seismic networks and spatial variations of completeness with high resolution (Schorlemmer & Woessner 2008). This method is based on the analysis of detection probabilities of seismic events and does not assume

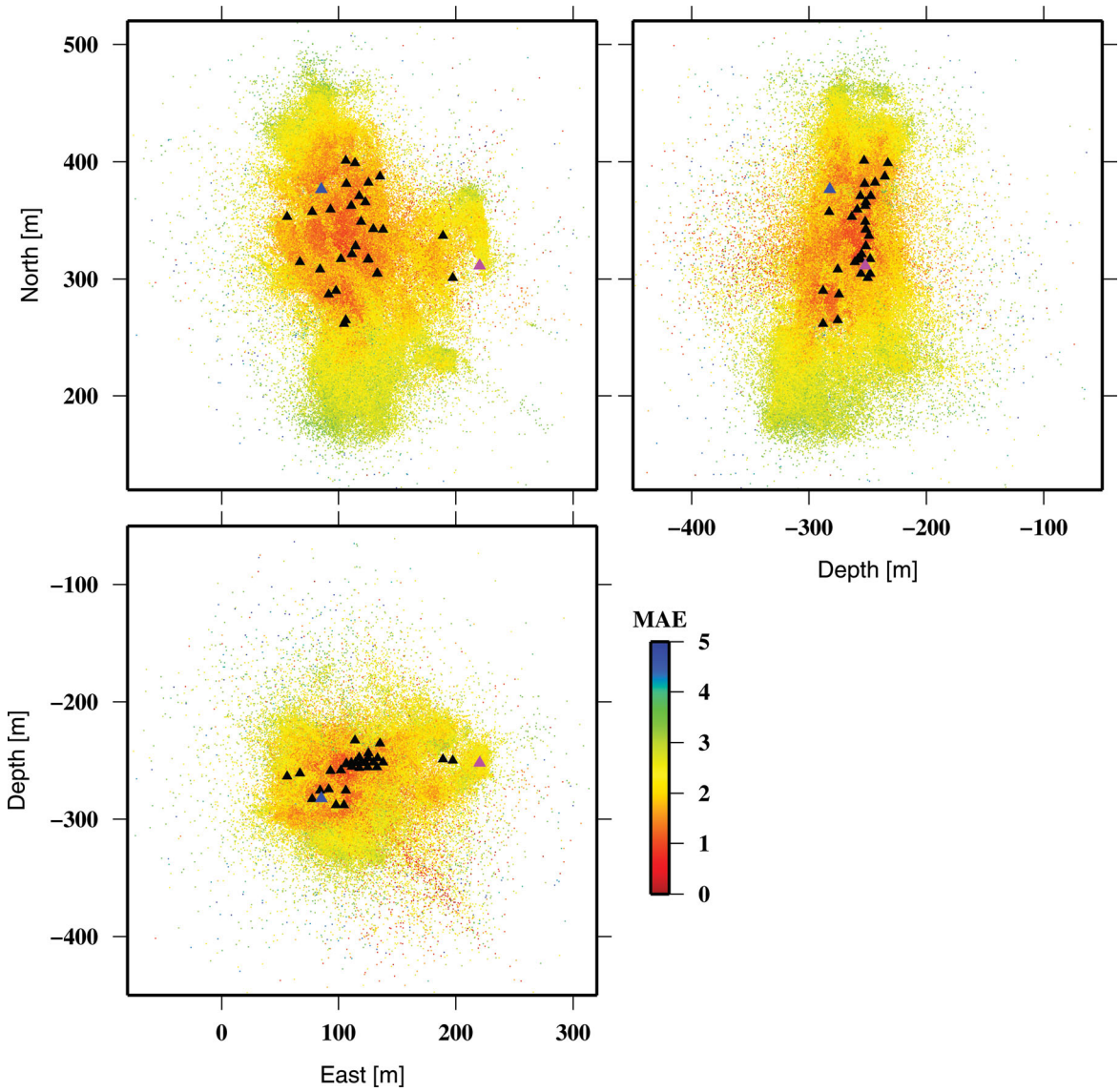

Figure 2. Hypocentral location of AE sources at Morsleben mine during the analysed 2 months period (2010 April–May): map view (up, left), NS-depth (up, right) and EW-depth cross-section (bottom, left) projections. The colour scale indicates the acoustic emission magnitude (M_{AE}) of the events, which is roughly equivalent to moment magnitudes M_w −8 to −3. Triangles denote sensor locations (blue and magenta triangles indicate stations 22 and 25).

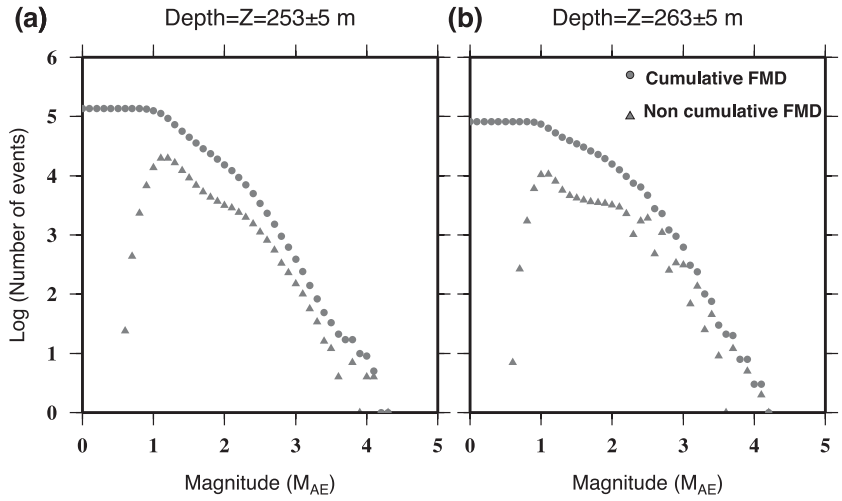

Figure 3. Frequency–magnitude distributions for all recorded data set within two depth profiles show that the FMD does not follow the Gutenberg–Richter power-law distribution.

a Gutenberg–Richter distribution of the earthquake catalogues. The analysis is performed in different steps (full details are given in Schorlemmer & Woessner 2008): first, the probability of detection is derived for each station in the network; then, the detection probabilities for different stations are combined into a probability of detection for the whole seismic network. In a last step, the spatial distributions of network detection probabilities are used to derive a map of completeness. This analysis was originally developed for regional seismic networks, covering an extension of hundreds of kilometres and being composed of surface stations (Schorlemmer & Woessner 2008; Nanjo *et al.* 2010) and depends only on magnitude, distance and time.

The PMC method uses the phase data, including earthquake catalogues, stations information and attenuation relations to determine magnitudes in the network. According to Schorlemmer and Woessner the detection probability $P_{D,i}(M,L)$ at a given station i is defined as a function of magnitude M and source–receiver distance L, as the ratio of the number of located events picked at this station over the overall number of events located by the network. The detection probability for a given earthquake with magnitude M at location x and for time t can be defined for a given station i as $P_{D,i}(M,x(L),t)$, where the effects of source–receiver geometry are only accounted by means of a distance L. Then, the detection probability of an event with magnitude M and given location x can be defined for the whole network, as the joint probability that a minimum number of stations have detected this event:

$$P_E(M, x, t) = f\left(P_{D,i}\left(M, x(L), t\right)\right). \tag{2}$$

The minimum number of stations must be adjusted to the triggering conditions of the network. The probabilistic magnitude of completeness (M_P) at location x and time t is derived by searching the smallest magnitude M that represents the desired probability of detection level (Schorlemmer & Woessner 2008):

$$M_P(M, x, t) = \min M \,|\, P_E(M, x, t) = 1 - Q\ , \tag{3}$$

where Q is the complementary probability that an event will be missed.

This approach may have strong limitations when analysing microseismicity in mining environments because of the 3-D network geometry and the presence of strong heterogeneities, including voids, galleries and different mineralogical units. To demonstrate the limitations of the standard PMC approach for our analysis, we compute the probability of detection depending on the direction of the source–receiver geometry (P_{DD}, where the second D index points out the 'directional' approach) for two sensors (sensor 25 and sensor 22). The P_{DD} is computed similarly to P_D, but only relying on events located above or below the sensor, respectively. Since most sensors are located at a cavity wall (often drilled at the cavity floor or ceiling) the probability to detect an earthquake may significantly differ if the wave fronts propagate down- or upward. Fig. 4 shows the non-smoothed detection probability for sensor 25 (top) and sensor 22 (bottom) with the standard approach, utilizing the whole catalogue as well as subsets containing only events above or below the sensors, respectively. The plots of detection probabilities show different patterns at the reference sensors, showing how sensor 22 has a better performance than station 25. In both cases, the detection probability estimated using the whole data set provided a different image than results from events located above and below the sensors. In particular, if we only consider events which are located below the sensors, the estimation of detection probabilities is much lower: for example, for station 25 at M_{AE} 2 and at a distance of 75 m, we obtain a detection probability of about 1.00 and 0.75, respectively, from the whole data set and the subcatalogue of events below the sensor. These results confirmed that the standard PMC method for

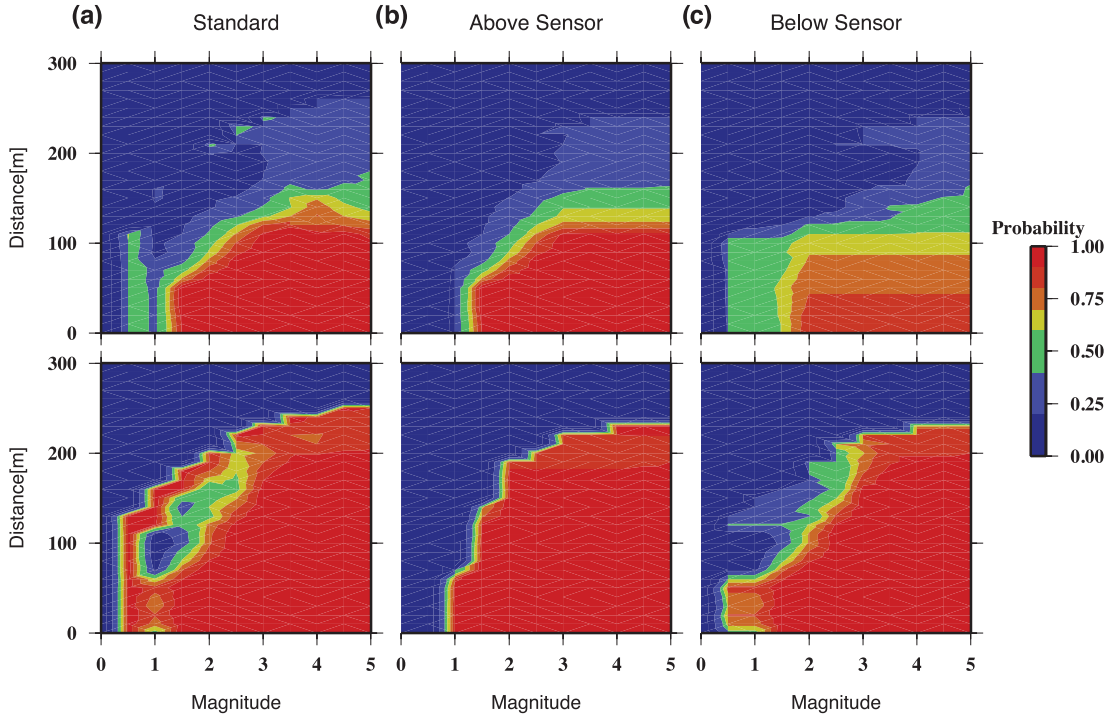

Figure 4. Probability of detection (P_D) at sensor 25 (top) and 22 (bottom) of the Morsleben network. P_D is plotted as a function of magnitude and distance. Three different plots are derived from (a) the whole data set, (b) using only events with depths shallower than the sensor's depth and (c) using only events with depths deeper than the sensor's depth.

mining networks, with detection probability only defined as a function of magnitude and distance, cannot provide stable estimations for probability of detection and magnitude of completeness. Because of these differences, and given the observed sensitivity to the direction of observation, we will further modify the PMC method based on the event magnitude, source–receiver distance and direction.

PROBABILITY OF DETECTION FOR MINING ENVIRONMENTS

Here, we describe our approach to extend the PMC method for heterogeneous media. The first goal is to derive the probability of earthquake detection at a specific sensor. Whereas in the standard PMC approach, this probability only depends on magnitude and distance, we additionally consider its dependency on the direction of the source location. To this purpose, we first define a number of preferential directions (N_d). Then, for each sensor the event detection catalogue is subdivided in N_d subcatalogues, each including only those events falling into the sector corresponding to its preferential direction. The choice of the number and orientations of preferential directions can be based on mining, geological and/or seismicity information of the study area. In our case, we choose two possible approaches for the Morsleben mine. In the first case, since most variations in the detection performance are observed between up- and downgoing wave fronts (likely as consequence of the installation of many sensors at gallery floor or ceilings), we subdivided the detection catalogues for each sensor into two subsets, one including all sources shallower than a given sensor and one with sources deeper than the sensor depth. In the second case, knowing the average orientation (N30W–S30E) of cavities, strike direction of the galleries and geological structures at this mine, we choose six preferential directions (up, down, N30W, N60E, S30E and S60W). An event is associated with one of the six preferential directions based on the maximum of the scalar product of the unit vector of the source–receiver direction with the unit vectors of the six preferential directions. The events classification into catalogue subsets for six preferential directions is illustrated in Fig. 5 for sensor 22. The method is very flexible because it allows choosing different configurations of the preferential direction, depending on the study case. Increasing the number of preferential directions would be useful to taking account local heterogeneities in study, however; results in smaller size of the catalogue subset and may not ensure a stable retrieval of the PMC. Note that our approach will provide a 3-D image of detection capability of each sensor, not limited to a specified depth.

Plenkers *et al.* (2011) derived detection probabilities of each sensor as a function of magnitude, distance and azimuth for specific depth ranges for a gold mine in South Africa. The general idea to derive the completeness in both studies is similar and focuses a similar problem, linked to heterogeneous media, where the standard PMC may fail. However, there are some significant differences between the study of Plenkers *et al.* (2011) and our approach. Although both studies rely on magnitude, distance and azimuth, in our approach we use preferential directions and split the catalogue into subcatalogues, with events falling into cones relative to each sensor. Note that the cone-like shape of the subregions allow the further application of the standard PMC analysis, describing the probability of detection of a sensor within each cone as a function of magnitude and distance. Because of this classification in few subcatalogues to provide prior information about heterogeneities, the computational expenses in our method are much smaller than the method of Plenkers *et al.* (2011). This is especially important where large monitoring areas need to be studied, for example, in commercial mines. Therefore we overcome problems related to sparse data in large areas and investigate the effects of missed/unlocated events on M_c estimations. A second difference concerns the data application, which here relies on a massive data set from the Morsleben network (more than one million events) and a dense network (including 32 sensors). Such optimal configuration is very important to detect cavity effects from different sides. Given our approach and data set, we are able to reconstruct a 3-D map of M_c.

For each catalogue subset, representing a specified preferential direction, we perform the PMC analysis as a function of magnitude and distance. Since we compute probabilities in a distance–magnitude space, we need to homogenize distance and magnitude units. To these purposes, we use the attenuation relation given for the network. The maximum amplitude decays as a function of distance between the AE source and the sensors and this behaviour is used to determine the event magnitude. Expressing the amplitude in dB, we have a linear decay of the maximum amplitude with distance, with the slope describing the damping coefficient (e.g. Manthei *et al.*

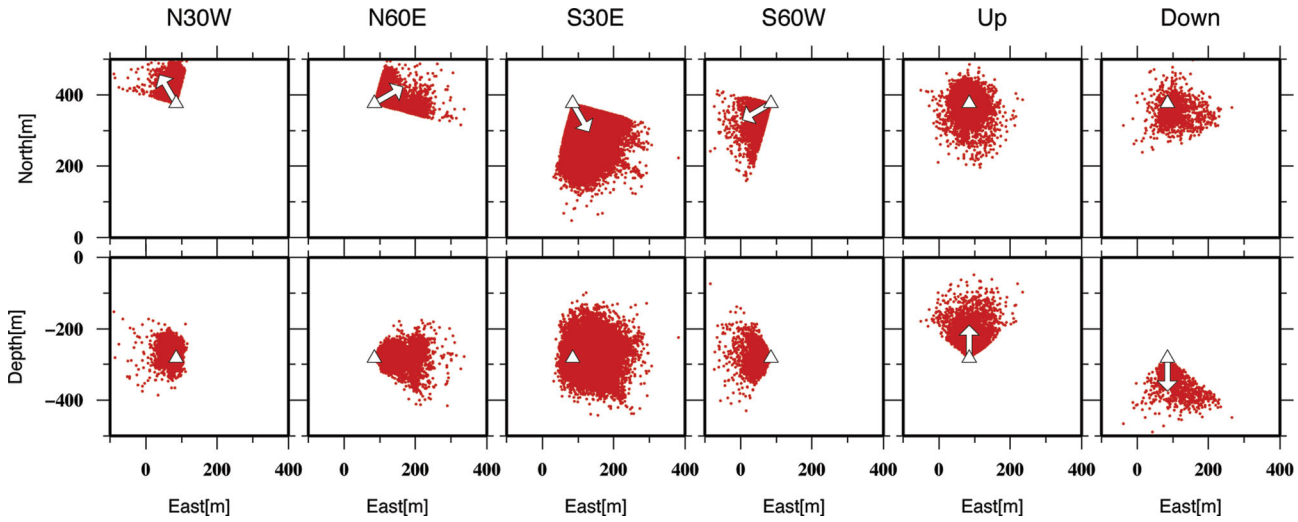

Figure 5. Example of derivation of six subcatalogues for six preferential directions (arrows) for seismic events recorded by sensor 22 (triangle) in the network. Top: map view of epicentral locations for six subcatalogues. Bottom: locations of the same events projected along an EW cross-section.

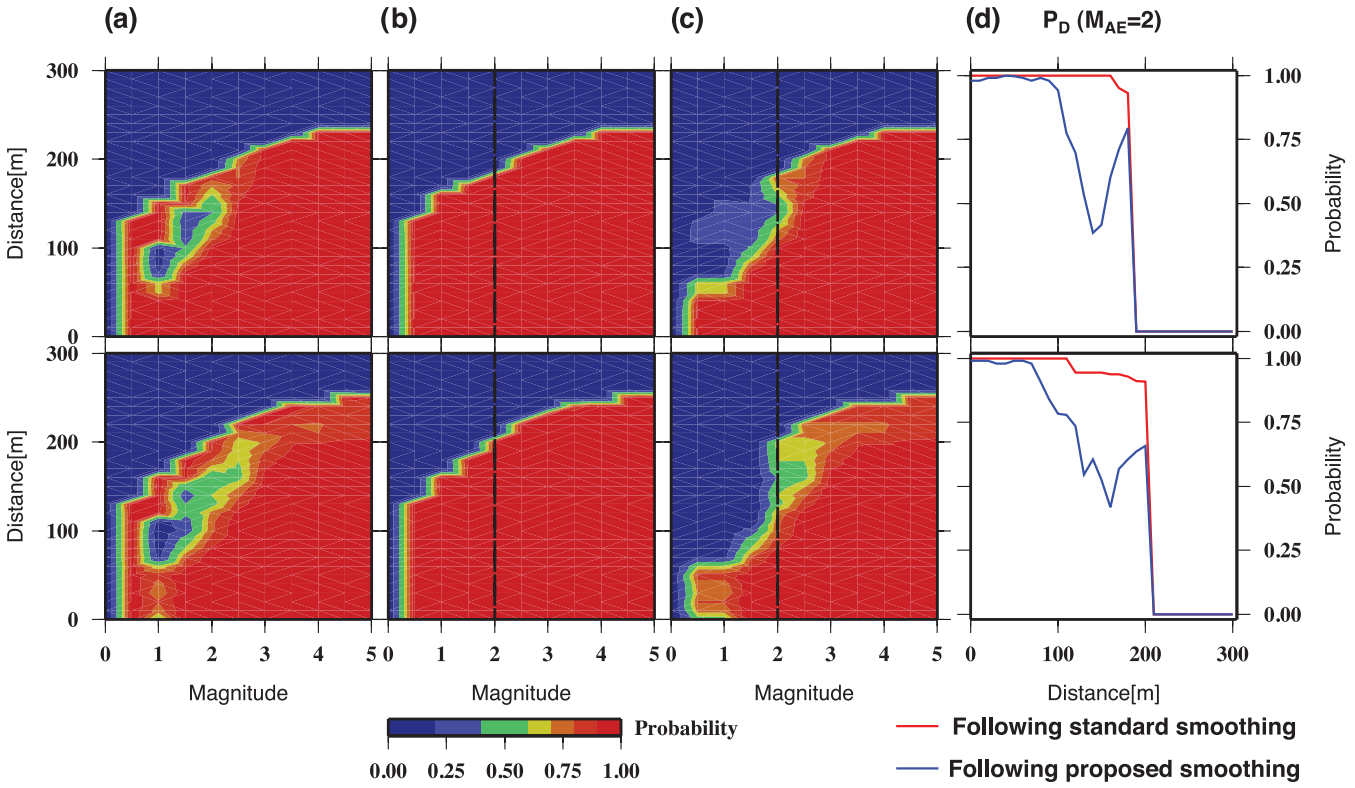

Figure 6. Probability of detection for sensor six (top) and sensor 22 (bottom) of Morsleben network, as a function of distance and magnitude, following the standard PMC approach. (a) Unprocessed results, (b) smoothed results according to Schorlemmer & Woessner (2008) and (c) smoothed results according to this study. (d) Probability as a function of distance for a magnitude $M_{AE} = 2$ (dashed black lines on the left plots), using the standard smoothing (red lines) and the smoothing proposed in this study (blue dashed lines). This figure shows the effects of different smoothing approaches: the method adopted in the standard PMC approach can hide anomalous distance-dependent detection pattern, which might be related to cavities and/or structural heterogeneities.

2006). Köhler *et al.* (2009) estimated a slope of (-0.26) dB m^{-1}. The event magnitude would then be defined from the amplitude expected for a reference distance of 50 m. According to the discussion on eq. (1), we use a fixed ratio of 20 to scale amplitudes to AE magnitudes. We can finally infer that a distance variation of 100 m, would imply an amplitude increase of 26 dB, and thus is equivalent to a magnitude variation of 1.3. This relation is used to define a Euclidian distance in the magnitude–distance space, and to convert data triplets to detection probabilities, according to Schorlemmer & Woessner (2008).

We define $P_{DD,ij}(M, L)$ as the detection probability for magnitude M and distance L at station i from preferential direction j. P_{DD} for each station and preferential direction will be defined consistently as in standard PMC, as the ratio between the number of triggers and the number of events. To derive the detection probabilities for events of given magnitude, distance and given preferential direction to sensor, we apply the same criterion as used in the standard PMC method by Schorlemmer & Woessner (2008). Because of the extremely high number of recorded events, we changed the original assumption for the sufficient number of events per bin and set it to 100. This leads to a more conservative and robust estimation of probabilities. Following our modifications, the detection probability for a given earthquake with magnitude M at location x (and for time t) will be defined for a given station i as $P_{DD,\,ij(x)}\,(M, x(L),t)$. Now, the effects of source–receiver geometry are considered in the choice of the closest preferential direction j and the distance L.

Schorlemmer & Woessner (2008) suggested two simple physical constraints to obtain a smoothed distribution for the probability of detection: the detection probability cannot decrease (1) at smaller distances for the same magnitude and (2) for larger magnitudes at the same distance. This smoothing algorithm was proposed to remove artefacts due to sparse data, and relies on reasonable assumptions, when dealing with seismic waveforms propagating in homogeneous media. However, this approach may hide features stemming from heterogeneities and cavity effects. For some sensors at the Morsleben mine, the probability of detection shows some anomalies with respect to this expected behaviour. For example, regions of low detection probabilities can be seen, in few cases, within regions of higher probabilities (Fig. 6). Following the smoothing approach, these features would be removed. However, in the case of mining networks, we believe they may be related to cavities and/or structural heterogeneities. Thus, we prefer to implement a different smoothing approach, which assumes that the detection probability cannot increase for smaller magnitude at the same distance, but does not assume that the detection probability must decrease with distance. An increment of detection probability with distance may occur, if a large cavity is present between the source and the receiver, in the region behind a cavity. This effect is discussed in the synthetic modelling section. Fig. 6 shows the examples of the detection probabilities for two sensors (six and 22) and the smoothed distributions resulting from both approaches. The differences among smoothed probabilities indicate that our choice is more conservative, because it accounts for the possible effects associated to structural heterogeneities or cavities. The problem is further discussed in the synthetic waveform modelling section.

In the second step, sensor detection probabilities are computed for a given magnitude at a given location for all sensors. This process is similar to the one proposed by Schorlemmer & Woessner (2008),

but it also relies on the sensor detection probabilities for different preferential directions. We can compute a detection probability map for the network, for a given magnitude. First, for each gridpoint, we compute the distance and direction to each sensor, and extract the probability of detection $P_{DD,ij}$ for the given magnitude, distance and preferential direction (closest to the sensor–grid vector). Then, the probabilities at all sensors are merged to estimate the network detection probability (P_{ED}). This step takes into account the minimum number of triggers, which are needed for the detection of an event (in the case of the Morsleben data set five station triggers are needed for event detection). The repeated computation for a full range of magnitudes (here $0 \leq M_{AE} \leq 5$) provides a description of detection probabilities for each grid cell and magnitude. These detection probabilities are used to derive the magnitude of completeness, by searching the smallest magnitude that reflects earthquake detection with the desired probability. The choice of Q reflects the desired accuracy. Since the choice of Q value is arbitrary, we test different Q values, and choose $Q = 0.001$ to obtain conservative estimates.

RESULTS

In the following, we estimate the spatial distribution of detection probabilities and magnitude of completeness for the Morsleben network using 10 m grid spacing in North and East at a horizontal depth section profile ($z = 253 \pm 5$ m) and an EW cross-section ($x = 85 \pm 5$ m) where the seismicity is more concentrated. First, we obtain the probability of detection at each station. Fig. 7 shows the detection probabilities for sensor 22 following the standard PMC approach and considering two (above and below the sensor) and six preferential directions. The differences observed between detection probabilities in different directions confirm once more the directional dependency of P_{ED}; for example, detection probabilities of this sensor are larger for events located towards South and above the sensor, rather than towards North and below it. The standard PMC tends, in this case, to overestimate the probability that events are detected; for example, an event with $M_{AE} = 3$ at 200 m distance has a detection probability of 92 per cent, whereas probabilities are always below 10 per cent, in our modified approach, except for events located towards S30E (71 per cent).

The results of the detection probabilities and magnitudes of completeness for the entire network (30 sensors are used, sensor 10 and 21 were removed due to a very low detection capability) are illustrated in Fig. 8, where detection probabilities are shown for M_{AE} 1.5, for one map view and a cross-section profile. Detection probabilities extracted from the standard approach of PMC and two-directions PMC show similar spatial distributions, although the second approach tends to identify a region of high probabilities more extend in North–South direction rather than East–West direction. The magnitude of completeness is plotted in Fig. 8 for a detection probability of 0.999. Standard and two-directional PMC approaches indicate a magnitude of completeness of $M_c \approx 0.5$ in a central region elongated in North–South direction; the magnitude of completeness rises (faster for the standard PMC than for the two-direction approach) when moving far from the network. In general, since detection probabilities and magnitude of completeness depend on the Euclidian distance between sensors and source, their estimations for different source depths will change.

Completeness distributions computed from PMC analysis considering six preferential directions for two profiles show a different pattern. Assuming again a reference magnitude of M_{AE} 1.5, for the depth section, high detection probabilities are only predicted for a small region, close to the network, compared to the two other approaches (standard PMC, depth-dependent PMC). The M_c estimate in the centre of the network is about $M_c \approx 1$ and increases up to $M_c \approx 4$ at the boundaries of the study region. At about 150 m from the centre of the network, the detection probability, even for the largest magnitude events in the catalogue, cannot reach the chosen threshold of 0.999. The cross-section plot illustrates that the detection probability is highest in a small region around the centre of the network and elongated below the sensors. Estimation of the completeness distribution along the EW cross section using a 10 m grid shows this region with high probabilities of detection and low magnitudes of completeness ($M_c \approx 0.5$) below the centre of the network. The small number of events (Fig. 2, right) recorded in this region may significantly affect the completeness estimation. M_c reaches up to about 1 at the centre of the network; M_c variations are minor along the NW–SE direction ($M_c \approx 0.5$–2.5), compared to the NE–SW direction ($M_c \approx 1$–4).

These results show that the detection performance of the Morsleben network changes strongly, when considering different hypocentral regions. Highest detection probabilities and lowest magnitudes of completeness are somehow confined to a smaller region, which extends along a NNW–SSE direction, rather than N–S; the NNW–SSE orientation corresponds to the strike of the salt structure in the region (e.g. Best 1996). A similar analysis at different depths consistently indicates such general pattern, with a region of low M_c elongated according to the salt body geometry.

EFFECTS OF A CAVITY ON SYNTHETIC WAVEFORMS AND DETECTION PROBABILITY

In this section we investigate the effects of the presence of cavities, in terms of detection probability and magnitude of completeness, with the simplified synthetic tests. In these simulations, we focus on the forward modelling in two dimensions. Qualitative results can be extrapolated to the 3-D case. Synthetic seismograms have been computed using the E3D code (Larsen & Grieger 1998). First, we consider a homogeneous 2-D medium ($V_p = 4.7\,\mathrm{km\,s^{-1}}$, $V_s = 2.7\,\mathrm{km\,s^{-1}}$, 2.5 g $\mathrm{cm^{-3}}$), choose a station location and iteratively estimate the maximal velocity for isotropic sources located at each possible location in the model. The entire model has a spatial extension of 1 × 1 km, with a grid step of 5 m. Synthetic velocity seismograms in the radial direction are estimated assuming an explosive point source. Results are shown for two different station locations in Fig. 9(a), where the scale refers to normalized amplitudes. In the case that the model is homogeneous, the amplitude decay is only dependent on the geometrical spreading and attenuation, and therefore the maximal amplitudes decay symmetrically in each direction away from the station. The maximal amplitude depends here only on the source–receiver distance.

In the second case, we include a rectangular cavity of 50 × 25 m. The cavity is located below the stations; the distances between the closest boundary and the two stations are 10 and 30 m. The patterns of the maximal amplitudes recorded at the two stations are highly affected by the presence of the cavity (Fig. 9a, right). While the cavity acts as a barrier for sources located below it, which are shadowed by its presence, the interference of direct and cavity reflected phase's increases the maximal amplitudes recorded for stations above the cavity. Such effect, however, is strictly related to the radiation pattern of the isotropic source we chose, and may significantly change when using a different focal mechanism.

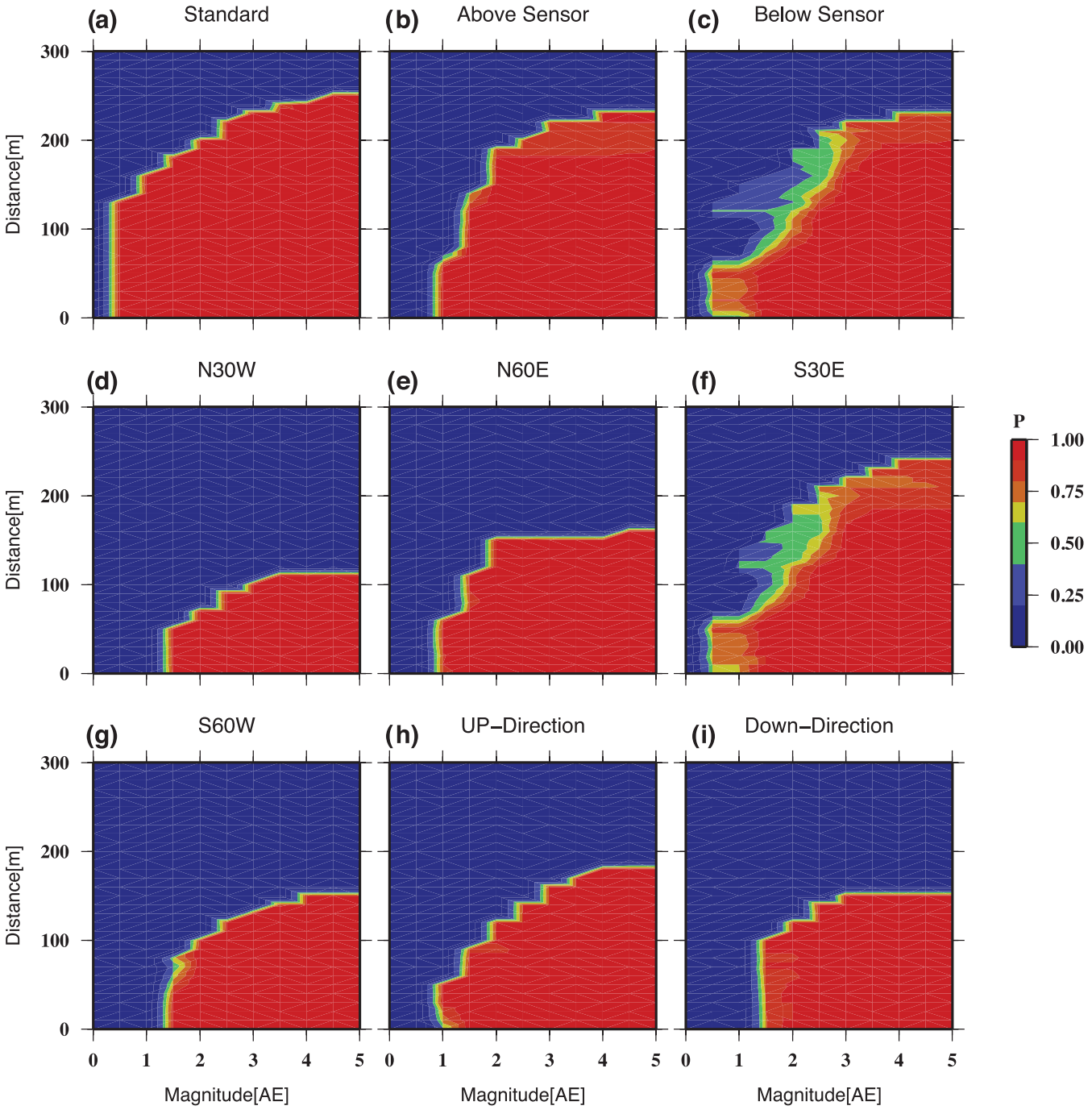

Figure 7. Probability of detection at sensor 22 as a function of magnitude and distance, as derived using three different approaches: (a) standard PMC approach based on the whole data set (b, c) modified PMC with two preferential directions (up, down), and (d–i) modified PMC with six preferential directions (up, down, N30W, N60E, S30E and S60W). The figure shows that detection probabilities for this sensor differ using events recorded in different subcatalogues. These differences are seen for all sensors and confirm that detection probabilities strongly depend on the direction of the source location.

The shadow effect of the cavity is stronger, when the station is closer to the cavity. Let us now assume that an event is detected at a station whenever the maximal amplitude is above a threshold, which is here chosen as the maximal amplitude recorded at a source–receiver distance of 75 m for an isotropic source with AE magnitude (M_{AE}) equal to 2.0. These are realistic values, defined after results obtained following the standard application of the probability of detection method to the Morsleben network. Since the maximal amplitude scales linearly with the scalar moment and thus exponentially with the magnitude, we can easily plot previous results in terms of the magnitude of completeness. The resulting M_c values are shown in Fig. 9(a), right-hand side, for all the four configurations discussed before.

Fig. 9(b) shows the variation of magnitude of completeness for both models along two profiles: AA′ (away from the receiver) and BB′ (constant distance to the receiver, variable direction). Along the AA′ profile, the homogeneous model predicts an increase of M_c for increasing distances. In presence of a cavity, results are significantly different: in front of the cavity, M_c estimation resembles the homogeneous case; while behind the cavity M_c values strongly

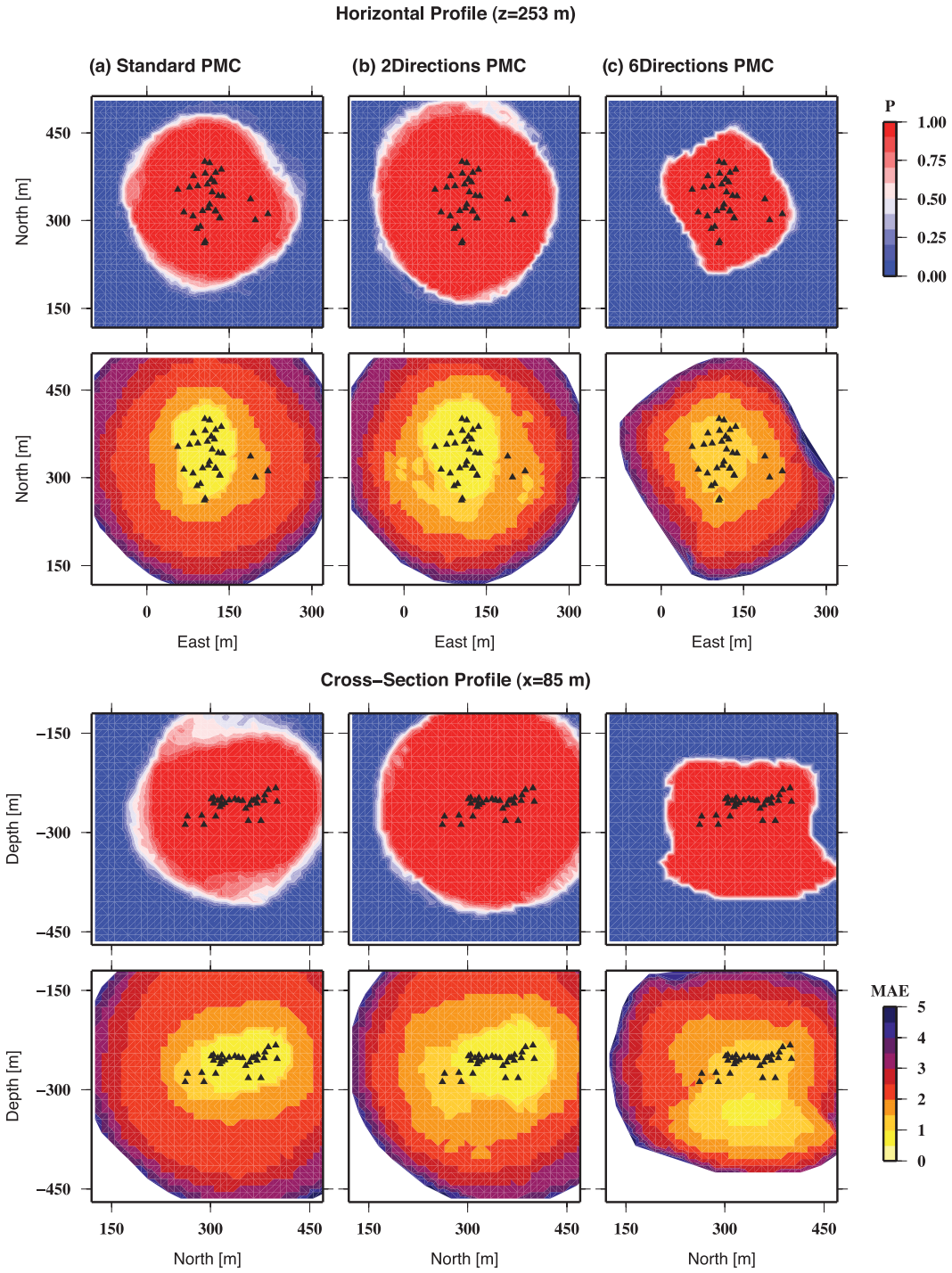

Figure 8. Spatial distribution of network detection probabilities (for a reference magnitude of M_{AE} 1.5) and magnitude of completeness for the Morsleben network using 10 m grid spacing along a depth section at $z = 253$ m (top) and a EW cross-section at $x = 85$ m (bottom). Black triangles are locations of working sensors. The figure show, according to colour scales, the probability and completeness maps using application of the standard PMC approach (a), modified PMC for up- and down directions (b) and for six preferential directions (c). Maps of completeness magnitudes are derived at the probability level of $P = 0.999$.

increase. The plot also shows that the magnitude of completeness is not always increasing when increasing the distance to the receiver. A higher magnitude of completeness can be derived close behind the cavity wall, where the shadow effect of the cavity is largest, while smaller M_c can be derived at further distances. This result confirms that the smoothing procedure, discussed in the methodology section, should not force the decrease of detection probability when increasing the source–receiver distance. The results along the BB′ profile show how the M_c is affected at the same source–receiver distance, when a cavity is located between source and receiver.

To verify the hypothesis that the distribution and geometry of cavities is linked to the patterns observed in the probability of detection at Morsleben, we compare theestimated probability of detection with the geometry of cavities. The test is realized again in two dimensions, and results interpretation must account for this simplified assumption. We consider station 22 of the Morsleben

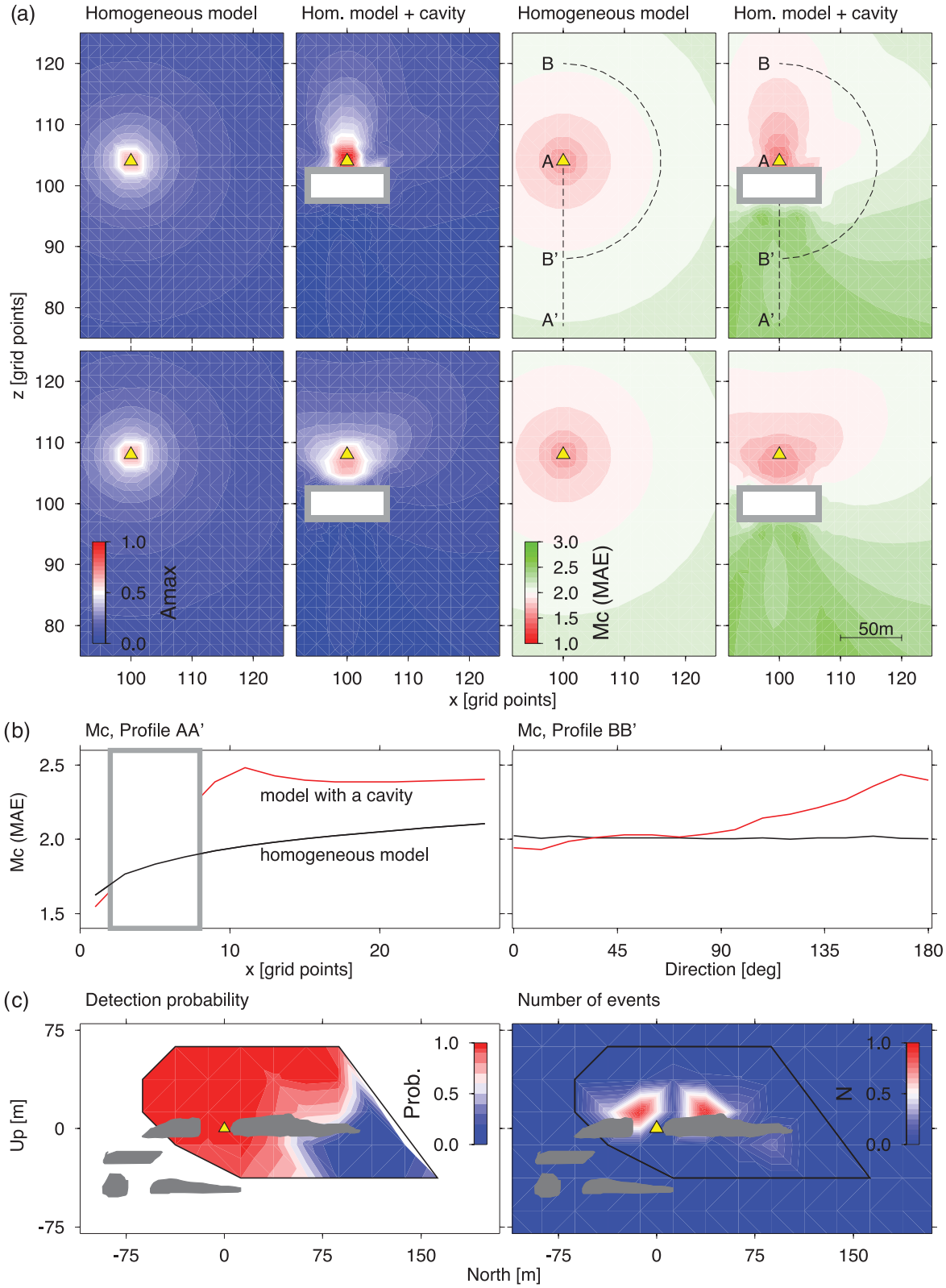

Figure 9. (a) Synthetic maximum amplitudes (normalized) calculated at a presumed station (triangle) for an isotropic source located at the corresponding gridpoint in the case of a homogeneous model without and with a rectangular cavity; right-hand side: magnitude of completeness (M_{AE}) at two stations (triangles) for a homogeneous model and a homogeneous model with a rectangular cavity; dashed lines denote profiles AA′ and BB′. (b) M_c along profiles AA′ (left) and BB′ (right), for a homogeneous model and a homogeneous model with a rectangular cavity (grey area). (c) Probability of detection (left-hand side) and normalized number of events (right-hand side) along a North–South cross-section at station 22.

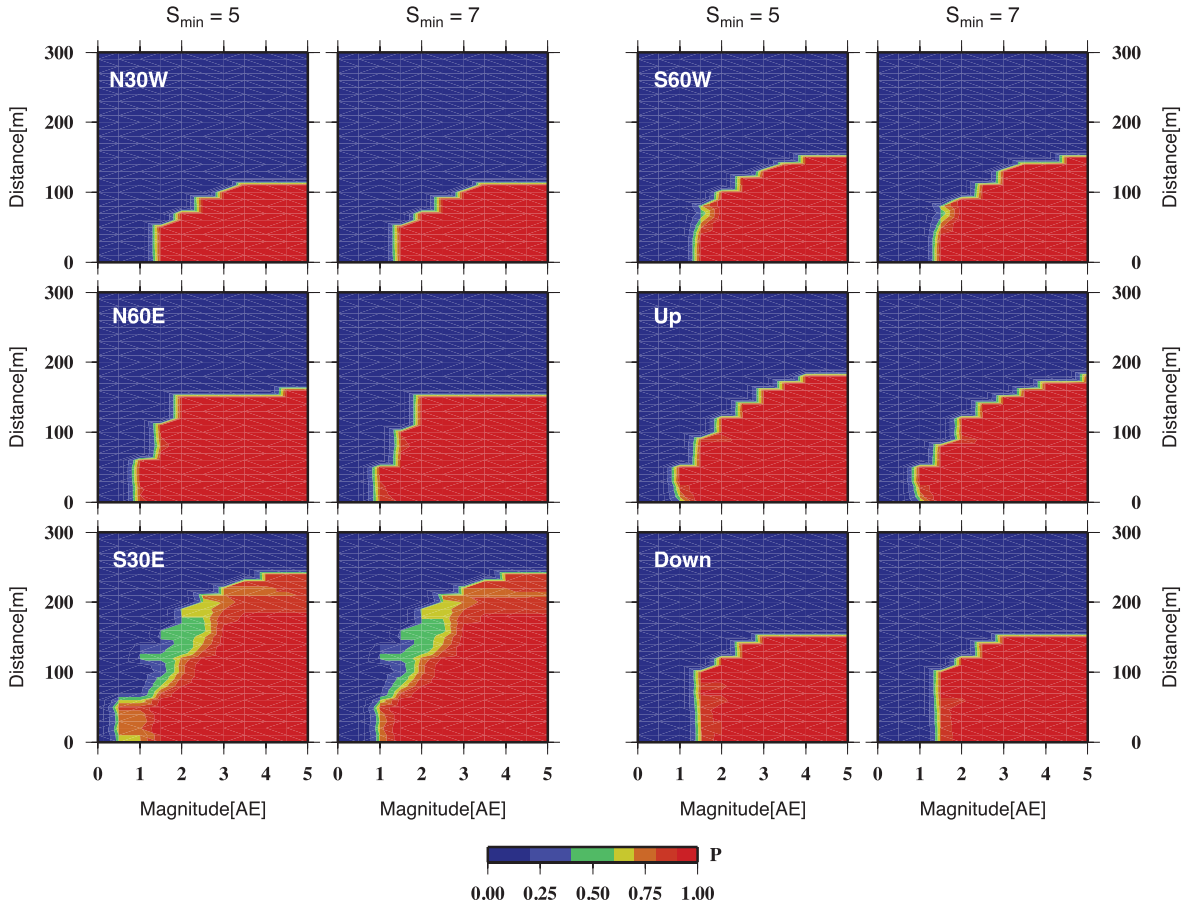

Figure 10. Effects of increasing the minimum number of required stations for locating events on the distribution of detection probabilities (P_D) for sensor 22 in different preferential directions (N30W, N60E, S30E, S60W, up and down). The first and third columns show P_D derived with a minimum number of five stations for locating events, columns second and forth with a minimum number of seven stations. Results show that the distribution of detection probabilities are not significantly affected when increasing the number of stations required for location.

network and consider all seismic events located in a North–South vertical section centred at this station (the E–W thickness of the section is 25 m and only events located in this 'slice' are considered). The section is divided in cells of 25 × 25 m, and at each cell the probability of detection at this single station (for events with M_{AE} 1.5 ± 0.5) is computed. Fig. 9(c, left-hand side) shows how the probability of detection decreases faster towards North, a pattern that can be explained as a consequence of the nearby cavity. It is important to point out that the spatial pattern of the detection probability is not related to the spatial distribution of events (Fig. 9c, right-hand side).

DISCUSSION

Detection probability distributions at Morsleben mine are computed based on the information of recorded and not-recorded *P* phases. Given the configuration of the Morsleben mine network, high traveltime residuals may be derived due to cavity effects, and consequently some events may be detected but not located, when the number of good traveltimes becomes too small. Therefore, the effects of missing and unlocated events should be considered in the PMC analysis.

To investigate the effects of missed and unlocated events on the detection probability distribution, we exploited the information about the stations used in the localization procedure. We increased the minimum number of required stations (S_{min}) for locating an event to seven stations (instead of five). Consequently, some events in each subcatalogues derived from different preferential directions will be missed. After increasing the minimum number of required stations for localization to seven, about 11 per cent of events are lost. As a typical example, we discuss here the effect on the probability distribution for station 22. Fig. 10 shows the differences between detection probabilities for the six preferential directions subcatalogues for sensor 22. The comparison between results shows that the differences in P_D are minor, and negligible when compared to the differences observed among P_D for different preferential directions. This test proves that missing and unlocated events are not affecting the results of P_D and completeness estimations.

Another point which can affect the estimation of the detection probabilities is the role of the attenuation relation in the network. As we discussed, the standard PMC approach estimates the same probability of detection for seismic waves from all directions for a specific station. This assumption leads to overestimated probabilities and is not reliable especially for networks located in strongly heterogeneous media which attenuation is anisotropic. Our approach, based on the direction of source location, provides us with results based on the (directional) differentiation of observation picks. High-frequency acoustic waves are differently attenuated in different geological structures, affected by shadowing effects due to cavities, and scattered at blocks of anhydrite, small clay layers or inclusions of gas or water which are embedded in most salt rock formation.

These effects may lead to higher attenuation for regions close to the cavities and weaker AE signals, with respect to those attenuated by undisturbed rock salt (Manthei *et al.* 2006). Considering different attenuation relations for signals recorded in different settings can improve the magnitude uncertainty in the analysis and consequently improve detection probabilities. However, considering the unknown boundaries of the attenuation anomalies, and the combined effects of different bodies (e.g. salt rock and anhydrite) and cavities, it is currently not possible to account for them in our approach. They could be considered by including a large number of preferential directions (e.g. ignoring any *a priori* information on the geometry of the mine), or following the approach proposed by Plenkers *et al.* (2011). Since most events are recorded in the direction of the salt body, one velocity model (consistent with the salt body) and one attenuation relation is used towards magnitude determination in the network. In the modified PMC method the effect of cavities and highly attenuating bodies is reflected in the decrease of the detection probability in the specific direction to a sensor. Another factor which may affect the detection probability of an AE sensor is its orientation and coupling with the hosting rock. On one side, piezoelectric sensor amplification is dependent on the direction of the incoming seismic wave and detection performance may change depending on the sensor orientation (Manthei *et al.* 2001). Also, the sensor coupling with the rock surface may affect the average detection rate, as confirmed by significant variations of the performance of adjacent sensors. However, according to Plenkers *et al.* (2011), effects related to sensors orientation may not have a strong influence on the detection probability, when compared to the influence of structural heterogeneities.

CONCLUSIONS

Reliable estimations of the magnitude of completeness, especially for networks in heterogeneous environments, provide valuable knowledge about earthquake statistics and allow a correct interpretation of seismic catalogues. In this work, we studied the spatial distribution of the magnitude of completeness at the Morsleben salt mine by adapting the PMC approach to account for different source–receiver directions. A first attempt in this direction has been done by Plenkers *et al.* (2011) for a significantly smaller data set in a South African gold mine. We extended this approach and tested it for the much larger data set of the Morsleben mine. Our method still relies on the detection capability of each single seismic sensor of a seismic network as the standard PMC, which was proposed for regional surface networks monitoring regions with minor structural heterogeneities. While the standard PMC approach can provide an overall detection capability for each sensor and the whole seismic network, it cannot account for effects related to structural heterogeneities and cavities. These effects are considered in our modified approach, and their importance is confirmed by the observation of significant variations in the detection probability when considering seismic events located in different directions to the same sensor. The modified PMC approach is suggested for large data sets, with strong heterogeneities and different geological structures, as they affect the wave attenuations to different stations and in along different paths. The information on anomalous detection performance could be used to infer the geometry of cavities or geological structure units. The suggested method could also be applied to larger scale settings where blocks with strongly different attenuation properties are in close contact as, for example, at some transform boundaries or in the case of a border between igneous and sedimentary rocks. A second application to tectonic events could be at subduction zones: deep and shallow events at the same distance to the sensors present very different waveforms, and thus the detection performance can change significantly. However, due to the introduction of subcatalogues representing the different preferential directions, a much larger data set than in the original approach is needed and thus the standard PMC will remain the method of choice whenever homogeneous or only moderately heterogeneous regions are studied. A synthetic test using waveform modelling confirms that the patterns observed in the detection analysis can be explained as consequence of heterogeneities and cavities near the sensors.

The modified PMC approach is flexible and can be adapted and applied to different mines based on the geometry of mining operations and structural details. The modified PMC method can provide an image of the spatial distribution of the magnitude of completeness. In addition, the method can be used to judge the network performance and evaluate future network configurations. The results of the modified PMC approach find that the region of lowest M_c at Morsleben mine extends along a NNW–SSE direction, consistently with the elongation of the salt body exhibiting low signal attenuation.

Temporal completeness variations can affect different data sets and this can be extremely important in mining environments. Temporal changes reflect a time-dependent ability of the network to detect events. A variation of the network configuration and the number of sensors can have a strong influence on the overall detection performance. Seismic noise has also an effect on the detection performance, and the reduced anthropogenic noise from working activity in the mine can explain the larger number of detections (for M_{AE} below 1) at Morsleben during weekends. In consequence of some activities in mining environments, for example, following excavations, refilling, blasting and mass shifts, the mine structure can change with time. Such activities (which were not performed for the time period discussed in this work) strongly change the mining structure and should be reflected in a variation of the network detection performance. The proposed modified PMC analysis could be iteratively repeated for different time intervals, to investigate possible changes in the mine structures.

ACKNOWLEDGEMENTS

We are thankful to the BGR and BfS for providing access to the AE data catalogues and monitoring information, and to Dr. J. Philipp for providing information on the acquisition system and data processing. We are grateful to Dr. K. Plenkers, Dr. G. Kwiatek, Dr. J. Woessner and an anonymous reviewer for useful comments and suggestions. Thanks to Mr. M. Powers, who kindly revised the English text. This project is funded by the MINE research project. The project MINE is part of the R&D Programme GEOTECHNOLOGIEN and is funded by the German Ministry of Education and Research (BMBF), grant of project BMBF03G0737A.

REFERENCES

Amorèse, D., 2007. Applying a change-point detection method on frequency-magnitude distributions, *Bull. seism. Soc. Am.,* **97,** 1742–1749.

Becker, D., Cailleau, B., Dahm, T., Shapiro, S. & Kaiser, D., 2010. Stress triggering and stress memory observed from acoustic emission records in a salt mine, *Geophys. J. Int.,* **182,** 933–948.

Behlau, J. & Mingerzahn, G., 2001. Geological and tectonic investigations in the former Morsleben salt mine (Germany) as a basis for the safety assessment of a radioactive waste repository, *Eng. Geol.,* **61,** 83–97.

Ben-Zion, Y. & Zhu, L., 2002. Potency-magnitude scaling relations for Southern California earthquakes with 1.0 < ML < 7.0, *Geophys. J. Int.,* **148,** F1–F5.

Best, G., 1996. Raft tectonics in Northern Germany: First results of the seismic investigations at the salt structure Oberes Allertal, *Z. dt. Geol. Ges,* **147,** 455–465.

Cao, A.M. & Gao, S.S., 2002. Temporal variations of seismic b-values beneath northeastern japan island arc, *Geophys. Res. Lett.,* **29,** 48, 1–3.

Cichowicz, A., Green, R. & Brink, A.v.Z., 1988. Coda polarization properties of high-frequency micro seismic events, *Bull. seism. Soc. Am.,* **78,** 1297–1318.

Cox, S.J.D. & Meredith, P.G., 1993. Microcrack formation and material softening in rock measured by monitoring acoustic emissions, *Int. J. Rock Mech. Min. Sci. Geomech. Abstr.,* **30,** 11–24.

Eisenblätter, J. & Spies, T., 2000. Ein Magnitudenmass für Schallemyssionsanalyse und Mikroakustik, Deutsche Gesellschaft für Zerstörungsfreie Prüfung, 12. Kolloquium Schallemission, pp. 29–41, Jena, (in German).

Federal Office for Radiation Protection, 2009. Endlager Morsleben: Stilllegung des Endlagers für radioaktive Abfälle Morsleben, *Bundesamt für Strahlenschutz (BfS),* Available at: http://www.bfs.de/en/endlager/endlager_morsleben (2012).

Gentili, S., Sugan, M., Peruzza, L. & Schorlemmer, D., 2011. Probabilistic completeness assessment of the past 30 years of seismic monitoring in northeastern Italy, *Phys. Earth planet. Inter.,* **186,** 81–96.

Gibowicz, S.J. & Kijko, A., 1994. *An Introduction to Mining Seismology,* Academic Press, San Diego, CA, 399 p.

Gutenberg, B. & Richter, C.F., 1944. Frequency of earthquakes in California, *Bull. seism. Soc. Am.,* **34,** 185–188.

Hanks, T.C. & Boore, D.M., 1984. Moment-magnitude relations in theory and practice, *J. geophys. Res.,* **89,** 6229–6235.

Köhler, N., Spies, T. & Dahm, T., 2009. Seismicity patterns and variation of the frequency-magnitude distribution of microcracks in salt, *Geophys. J. Int.,* **179,** 489–499.

Kwiatek, G., Plenkers, K. & Dresen, G., 2011. Source parameters of picoseismicity recorded at Mponeng deep gold mine, South Africa: implications for scaling relations, *Bull. seism. Soc. Am.,* **6,** 2592–2608.

Larsen, S. & Grieger, J., 1998. Elastic modeling initiative: III, 3D computational modeling, *Soc. Explor. Geophys. Conference Proceeding,* **68,** 1803–1806.

Manthei, G., Eisenblätter, J. & Dahm, T., 2001. Moment tensor evaluation of acoustic emission sources in salt rock, *Constr. Build. Mater.,* **15,** 297–309.

Manthei, G., Eisenblätter, J. & Spies, T., 2006. Experience on acoustic wave propagation in rock salt in the frequency range 1–100 kHz and conclusions with respect to the feasibility of a rock salt dome as neutrino detector, *Int. J. Modern Phys. A,* **21,** 30–34.

Maxwell, S. & Young, R.P., 1998. Propagations effects of an underground excavation, *Tectonophysics,* **289,** 17–30.

Milev, A.M. & Spottiswoode, S.M., 2002. Effect of the rock properties on mining induced seismicity around the Ventersdorp Contact Reef, Witwatersrand Basin, South Africa, *Pure appl. Geophys.,* **159,** 165–177.

Nanjo, K.Z., Schorlemmer, D., Woessner, J., Wiemer, S. & Giardini, D., 2010. Earthquake detection capability of the Swiss Seismic Network, *Geophys. J. Int.,* **181,** 1713–1724.

Plenkers, K., Schorlemmer, D. & Kwiatek, G. the JAGURAS Group, 2011. On the probability of detecting Picoseismicity, *Bull. seism. Soc. Am.,* **101,** 2539–2591.

Preuss, J., Eilers, G. & Mauke, R., 2002. Post Closure Safety of the Morsleben Repository, WM'02 Conference, February 24–28, 2002, Tucson, AZ.

Rydelek, P.A. & Sacks, I.S., 1989. Testing the completeness of earthquake catalogs and the hypothesis of self-similarity, *Nature,* **337,** 251–253.

Schorlemmer, D., 2009. Probabilistic seismic network completeness: Theory, application and results (abstract), *Seismol. Res. Lett.,* **80,** 298.

Schorlemmer, D. & Woessner, J., 2008. Probability of detecting an earthquake, *Bull. seism. Soc. Am.,* **98,** 2103–2117.

Schorlemmer, D., Mele, F. & Marzocchi, W., 2010b. A completeness analysis of the national seismic network of italy, *J. Geophys. Res.,* **115,** B04308, doi:10.1029/2008JB006097.

Spies, T. & Eisenblätter, J., 2001a. Acoustic emission investigation of microcrack generation at geological boundaries, *Eng. Geol.,* **61,** 181–188.

Spies, T. & Eisenblätter, J., 2001b. Acoustic emission monitoring of closely spaced excavations in an underground repository, *J. acoust. Emission.,* **19,** 153–161.

Spies, T., Hesser, J., Eisenblätter, J. & Eilers, J., 2005. Measurements of acoustic emission during backfilling of large excavations, in *Proceedings of the 6th Symposium on Rock Bursts and Seismicity in Mines,* pp. 379–384, eds Potvin, Y. & Hudyman, M., Perth, Australia.

Wiemer, S. & Wyss, M., 2000. Minimum magnitude of completeness in earthquake catalogs: examples from Alaska, the Western United States & Japan, *Bull. seism. Soc. Am.,* **90,** 859–869.

Woessner, J. & Wiemer, S., 2005. Assessing the quality of earthquake catalogues: estimating the magnitude of completeness and its uncertainty, *Bull. seism. Soc. Am.,* **95,** 684–698.

Wyss, M., Hasegawa, A., Wiemer, S. & Umino, N., 1999. Quantitative mapping of precursory seismic quiescence before the 1989, M 7.1 off-Sanriku earthquake, Japan, *Ann. Di Geofis.,* **42,** 851–869.

Zuniga, R. & Wyss, M., 1995. Inadvertent changes in magnitude reported in earthquake catalogs: influence on b-value estimates, *Bull. seism. Soc. Am.,* **85,** 1858–1866.